Nanoscale

PAPER

View Article Online
View Journal | View Issue

Check for updates

Cite this: *Nanoscale*, 2024, **16**, 14350

Sculpting liquid metal stabilized interfaces: a gateway to liquid electronics†

Reek Mahapatra,[a] Subhabrata Das,[b] Arshdeep Kaur Gill,[a] Devender Singh,[a] Anvi Sangwan,[a] Kaushik Ghosh [b] and Debabrata Patra *[a]

Received 28th April 2024,
Accepted 27th June 2024

DOI: 10.1039/d4nr01836b

rsc.li/nanoscale

Liquid electronics have potential applications in soft robotics, printed electronics, and healable electronics. The intrinsic shortcomings of solid-state electronics can be offset by liquid conductors. Alloys of gallium have emerged as transformative materials for liquid electronics owing to their intrinsic fluidity, conductivity, and low toxicity. However, sculpting liquid metal or its composites into a 3D architecture is a challenging task. To tackle this issue, herein, we explored the interfacial chemistry of metal ions and tannic acid (TA) complexation at a liquid–liquid interface. First, we established that an M^{III}–TA network at the liquid–liquid interface could structure liquid in liquid by jamming the interfacial film. The surface coverage of the droplet largely depends on the concentration of metal ions, oxidation state of metal ions and pH of the surrounding environment. Further extending the approach, we demonstrated that TA-functionalized gallium nanoparticles (Ga NPs) can also sculpt liquid droplets in the presence of transition metal ions. Finally, a mold-based free-standing 3D architecture is obtained using the interfacial reaction and interfacial crowding of a metal–phenolate network. Conductivity measurement reveals that these liquid constructs can be used for low-voltage electronic applications, thus opening the door for liquid electronics.

Published on 29 Juuni 2024. Downloaded on 08/08/2025 06:59:17.

Introduction

Liquid electronics is still in its infancy but has the potential to change the face of electronics at its core.[1] It addresses the longstanding problem of recyclability and reconfigurability of solid-state electronic components. The ever-increasing demand for liquid electronics in various emerging fields, such as soft robotics,[2] wearable electronics,[3] energy storage,[4] sensors[5] and human–machine interfaces,[6] emphasizes the designing of electronic components and materials in their liquid form. It includes conductive, semiconductor and dielectric liquids, each tailored for specific applications.[7–9] Liquid metals with metallic conductivity and room temperature fluidity are prime candidates for liquid electronics.[10–12] Unlike Hg and other liquid metals, alloys of Ga have low toxicity and have emerged as potentially transformative materials for next-generation electronics.[13–15]

Shaping liquid metals in a pre-defined structure is the gateway to liquid electronics.[16] A recent study focused on the direct deposition of liquid metals on a target surface *via* 3D printing, spray printing and transfer printing.[17] Another strategy involves transferring liquid metal circuits on a deformable substrate to 3D surfaces.[18] However, most of these methods require sophisticated apparatus or custom masks, resulting in high processing costs and intricate preparation procedures. Thus, an easy approach with minimally modified processing steps is still required to print liquid metals. In this pursuit, liquid-in-liquid 3D printing may show a promising avenue, where liquid structures are stabilized *via* interfacial films or interfacial jamming[19] of surface-active materials at the liquid–liquid interface. This strategy uses low viscous immiscible liquids to create all-liquid constructs.[20] Implementing the aforementioned approach requires appropriate surface functionalization of liquid metal or liquid metal-based composites that could spontaneously self-assemble and create a robust network at the interface. Despite the unique features of liquid metals, their limited surface functionality, unpredictable reactivity and uncontrolled surface hydrophilicity limit their role as surface active materials.[21] Thus, a general surface coating that can strongly adhere to liquid metal surfaces and possibly form a stable interfacial film when self-assembled at the interface is highly sought after for liquid–liquid sculpting.

In this view, we were inspired by a naturally abundant polyphenol, tannic acid (TA),[22] owing to their natural abundance and universal surface adhesion.[23] TA, a polydentate ligand,

[a]*Energy and Environment Unit, Institute of Nano Science and Technology, Knowledge City, Mohali, Punjab, India. E-mail: patra@inst.ac.in*
[b]*Quantum Materials and Device Unit, Institute of Nano Science and Technology, Knowledge City, Mohali, Punjab, India*

† Electronic supplementary information (ESI) available. See DOI: https://doi.org/10.1039/d4nr01836b

This journal is © The Royal Society of Chemistry 2024

Published on 29 Juuni 2024. Downloaded on 08/08/2025 06:59:17.

forms coordination complexes with metal ions, and self-assembly of these complexes has been exploited for material-independent coating of functional materials. In the current study, we established that a metal–phenolic network at a liquid–liquid interface can be utilized to create non-equilibrium droplet shapes *via* the interfacial jamming of the film. The surface coverage of the droplets can be tuned by varying the concentration of the transition metal ions. The pH and redox responsiveness nature of the interfacial film was demonstrated macroscopically by analysing the surface coverage of the droplet. Later, the scope of this chemistry was further extended to assemble TA-functionalized Ga NPs at a liquid–liquid interface, and subsequent jamming of the interfacial film produced droplets of various non-equilibrium shapes. Finally, we unveiled mold-based all-liquid 3D molding to create arbitrary architectures stabilized by the Ga NP-TA network. The conductivity of the self-standing printed structure was demonstrated by measuring the current up to 5 μA at an applied potential of ±3 volts, thus opening up the possibility for low-voltage electronic applications.

Results and discussion

Initially, we focused on investigating the supramolecular complexation behaviour between TA and metal ions (M^{III}) at the liquid–liquid interface (Fig. 1a). For this purpose, several metal complexes, such as iron(III) acetylacetonate [$Fe(acac)_3$], manganese(III) acetylacetonate [$Mn(acac)_3$] and cobalt(III) acetylacetonate [$Co(acac)_3$], were chosen because of their solubility in the oil phase. The TA solution was prepared separately in water and was used as an aqueous phase. We anticipated that the biphasic system would result in the rapid formation of a metal (M^{III})–TA complex that would stabilize the oil–water interface (Fig. 1b; see also ESI, Fig. S1†). In the complex, the pyrogallol (1,2,3-trihydroxybenzene) moiety in TA acts as a bidentate ligand for M^{III} ions and forms bis and tris complexes.[24] The kinetics of the self-assembly of different metal ions with TA at the oil–water interface was monitored by measuring the dynamic interfacial tension using a pendant drop tensiometer. In our first experiment, a TA (1 mg mL^{-1})/$Fe(acac)_3$ (1 mM) pair was used to form a metal–phenolate network at the interface. The interfacial tension of $Fe(acac)_3$ in DCB (dichlorobenzene) with pure water was ~35 mN m^{-1}, which was very close to the interfacial tension of the DCB/water system (~37.2 mN m^{-1}). This implies that the metal complex alone could not provide stability to the interface. The interfacial tension of the TA/DCB system was found to be ~23 mN m^{-1}, suggesting the amphiphilic nature of the polyphenols. However, in the case of the TA/$Fe(acac)_3$ system, the equilibrium interfacial tension was further decreased to 18 mN m^{-1}, indicating the formation of a network at the oil–water interface.

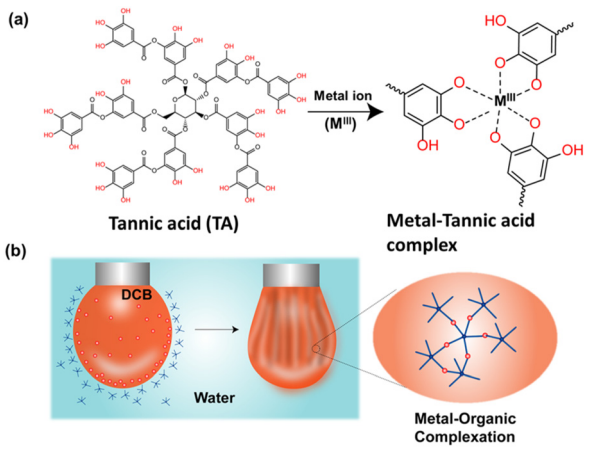

Fig. 1 (a) Chemical structure of TA and M^{III}–TA complexation. (b) Schematic representation of M^{III}–TA complexation at the oil–water interface.

Then, we were intrigued to explore the interfacial assembly of other metal ion variants, such as $Mn(acac)_3$ and $Co(acac)_3$, with TA. The interfacial assembly of $Mn(acac)_3$ exhibited similar behaviour to $Fe(acac)_3$, with a decrease in interfacial tension to 18 mN m^{-1}, suggesting the formation of a metal–organic complex. However, the decrease in interfacial tension observed with $Co(acac)_3$ was not as pronounced as with previously used metal ions, measuring ~22 mN m^{-1} (Fig. 2a). This indicates that the assembly of the $Co(acac)_3$ complex at the interface was less significant compared to the previously used metal salts. After establishing the robust interfacial assembly, we attempted to sculpt the droplet into various non-equilibrium shapes. In this experiment, a pendant drop of the oil solution containing metal ions was created by a syringe inside a cuvette containing the TA solution. After aging the droplet for 1200 s, a compressive force was applied to the Fe^{III}–TA assembly by reducing the volume of the droplet. This led to the formation of wrinkles, implying the transition from "liquid-like" assembly to "solid-like" assembly of the metal–phenolate network at the interface (see ESI SV1†). To prove the reversible nature of this jamming transition, the droplet was completely squeezed until it crumbled, but it returned to its initial shape after reinjection of the oil solution (Fig. 2b). This process was repeated numerous times on the same drop without any fracture or fatigue of the interfacial films. The same experiment was conducted with two other metal ions. Mn^{III} showed almost similar behaviour to Fe^{III} (see ESI SV2†). In the case of the Co^{III} ions, no significant jamming was observed because it did not form a stable complex with TA, thus validating the previous observation (see ESI SV3†). Next, we estimated the packing density of the interfacial film, and it was calculated from the ratio of V_w/V_i, where V_i was the initial volume of the droplet and V_w was the volume when the wrinkles started to appear on the interfacial film. Fig. 2c demonstrates that the surface coverage was 100% for both Fe^{III} and Mn^{III} in previously stated concentrations.

Because surfactant concentration plays an important role in stabilizing the interface, we were curious about investigating the effect of metal ion concentration on interfacial tension and surface coverage of the droplets. This was performed by

Published on 29 Juuni 2024. Downloaded on 08/08/2025 06:59:17.

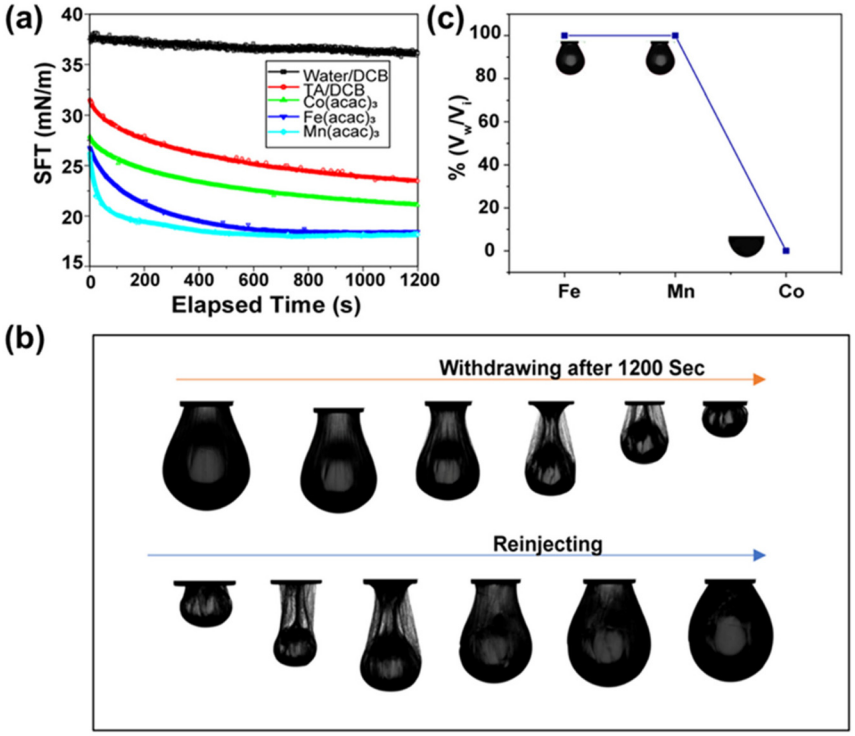

Fig. 2 (a) Time evolution of interfacial tension of TA and M^{III}–TA complexes. (b) Snapshot showing droplet morphology during the withdrawing and reinjection processes. (c) Surface coverage of the pendant droplets with TA (1 mg mL^{-1}) and M^{III} ions (1 mM).

varying the metal ion concentration from 0.1 mM to 1.0 mM, whereas the concentration of the TA was kept constant at 1 mg mL^{-1}. As the concentration of metal ions increased, a greater number of M^{III}–TA complexes were formed at the oil–water interface. This resulted in the lowering of interfacial tension and the enhancement of surface coverage. The results in Fig. 3a show that interfacial tension began to decrease with higher concentrations of metal ions. For Fe^{III} ions, the equilibrium interfacial tension gradually decreased from 23.4 mN m^{-1} to 18.45 mN m^{-1} as the concentration increased from 0.1 mM to 1 mM. A similar trend of interfacial tension was observed for Mn^{III} ions (Fig. 3b). It was evident that the surface coverage was also largely dependent on the concentration of metal ions. At the initial concentration of 0.1 mM Fe^{III}, the surface coverage was only 20%. It started to increase with a higher concentration of metal ions, *i.e.*, the surface coverage was 75% in the presence of 0.25 mM Fe^{III} and it reached 100% at 1 mM FeIII concentration (Fig. 3c). Similarly, the surface coverage increased from 20% to 100% when the concentration of Mn^{III} was changed from 0.1 mM to 1 mM (Fig. 3d).

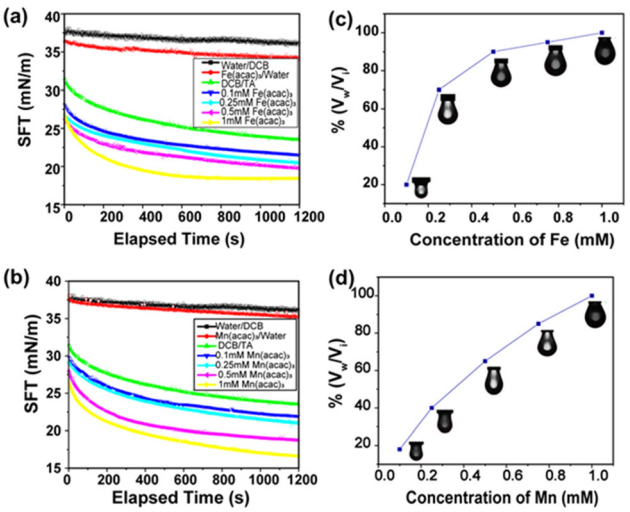

Fig. 3 (a) Time evolution of interfacial tension of TA (1 mg mL^{-1}) with varying Fe^{III} concentration and (b) TA (1 mg mL^{-1}) varying Mn^{III} concentration. (c) Surface coverage of TA (1 mg mL^{-1}) with varying Fe^{III} concentration and (d) TA (1 mg mL^{-1}) with varying Mn^{III} concentration.

Further, the interfacial assembly of the M^{III}–TA complex was investigated as a function of pH. TA possesses multiple hydroxyl groups that are coordinated to M^{III} *via* phenolate ions at basic pH.[25] The protonation of phenolate ions occurred at acidic pH, and their coordination stoichiometry with M^{III} was changed from a tris- to bis- to mono-coordinated state. Consequently, rapid disassembly of the interfacial film was also reflected in the surface coverage. At pH 1, the assembly of metal ions at the interface was minimal, with a surface coverage of only 20%, as shown in ESI (Fig. S2a†). However, as the pH was increased to 2, we witnessed a significant improvement in surface coverage, reaching nearly 80%. By further increasing the pH, we observed an enhancement in surface coverage,

 This journal is © The Royal Society of Chemistry 2024

Published on 29 Juuni 2024. Downloaded on 08/08/2025 06:59:17.

reaching up to 95% at pH 8. This increase in surface coverage was accompanied by a reduction in surface tension. Interestingly, by increasing the pH, we observed a corresponding enhancement in surface coverage and a decrease in surface tension (see ESI, Fig. S2b†).

Next, we investigated the role of the oxidation state of metal ions in the interfacial assembly of the TA. Fe^{III}, a hard Lewis acid, forms a stronger complex with TA due to the presence of negatively charged phenolate ions. However, in its reduced form, Fe^{II}, a borderline Lewis acid, has less affinity towards phenolate ions, thus forming a less stable complex with TA. Following this concept, we studied the reductive disassembly of the Fe^{III}–TA complex using ascorbic acid.[26] It is a well-known reducing agent that can easily convert Fe^{III} to Fe^{II}. In this experiment, a pendant drop containing an organic solution of $Fe(acac)_3$ (1 mM in DCB) was created into an aqueous solution of TA (1 mg mL^{-1}). As expected, interfacial assembly was easily formed at the interface, and the droplet was jammed after volume compression. Now, with the addition of ascorbic acid to the aqueous phase, the jammed droplet returned to its original shape (see ESI, Fig. S3†). No further jamming occurred upon further volume compression. This implies that the interfacial assembly was disintegrated due to a change in the oxidation state of the metal ions.

Inter-cellular communication is a hallmark of living systems.[27] The transport of signaling substances across the cell membrane is crucial for communication.[28] In this regard, droplets can serve as minimalistic models where the gated diffusion through the interfacial membrane can be examined to gain a perspective on pore-driven communication. To understand the inter-droplet communication through pores, we created two droplets stabilized by the M^{III}–TA complex at the interface. Usually, when two droplets of the same liquid or miscible liquid are in contact with each other, they merge to minimize interfacial tension. Merging can be hindered by creating an elastic film at the interface between droplets. We observed the same when two droplets containing metal–phenolate films at the interface were brought into contact with each other (see ESI, Fig. S4†). Next, we were intrigued to know if there was any communication between the two non-merging droplets. To achieve this goal, we choose a polymerization reaction of dicyclopentadiene (DCPD) in the presence of Grubbs catalyst (see ESI, Fig. S5†).

These reactants were soluble in organic solvents; thus, they were taken separately inside the two droplets. We assume that the rapid kinetics of ring opening metathesis polymerization (ROMP) would enable us to visualize the communication between droplets. In this study, one droplet containing DCPD monomer was placed above another droplet containing Grubbs catalyst, and the experiment was conducted inside a cuvette filled with a TA solution. Once these two distinct droplets were kept in contact, their contents started to communicate through the pores of the interfacial films. This initiated the ROMP, and a polymeric network began to form between the droplets. This process occurred within a brief span of merely 30 s, and the droplets merged into a single cohesive entity (Fig. 4a). This clearly indicates that the two non-merging droplets were able to communicate through pores when they were in contact with each other. Next, we attempted to block communication between the droplets by jamming the droplets containing the DCPD monomer. We observed that the droplets did not merge upon contact for 30 s (Fig. 4b). Thus, it was confirmed that the jamming of droplets shut down the pores of the interfacial film, which allowed communication between neighboring droplets.

The ability to structure a low viscous liquid inside another immiscible low viscous liquid is a challenging task. It requires a stable elastic film at the interface that can hold the structure in a non-equilibrium shape. In this context, the elastic nature of the metal–phenolate interfacial films comprising TA-coated functional nanomaterials can be utilized to sculpt liquid inside the liquid. It would also impart nanomaterial-derived functionality to all liquid systems. To demonstrate this concept, we chose liquid metal nanoparticles that could be further used for liquid electronics applications. TA-functionalized Ga NPs were synthesized using the probe sonication method (Fig. 5a). The sonication resulted in the oligomerization of TA, which stabilized the smaller Ga NPs.[29] The size and morphology of the freshly prepared NPs were examined under electron microscopy. The scanning electron microscope (SEM) images revealed spherical NPs with diameters ranging from 40 nm to 250 nm (Fig. 5b). The NPs were further examined using a transmission electron microscope (TEM), and micrographs revealed a core–shell structure confirming the presence of TA coating around Ga NPs. The particle diameter matched closely with the previous observation, and the coating thickness was found to be ~13 nm (see ESI, Fig. S6†). Later, energy-dispersive X-ray spectroscopy (EDX) mapping confirmed the presence of Ga and organic contents in the functionalized Ga NPs (Fig. 5c). Fourier transform infrared (FTIR) spectroscopy was used to investigate the chemical interactions between the TA and Ga NPs (Fig. 5d). This revealed that the phenolic C–O stretching bands of TA at 1533 and 1440 cm^{-1} were shifted to 1505 and 1378 cm^{-1}, respectively. Another significant change

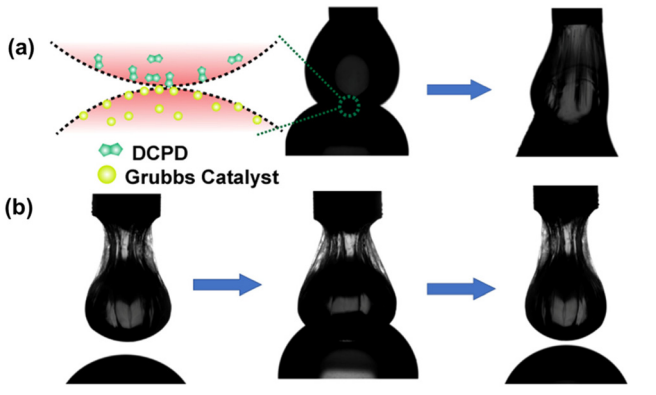

Fig. 4 (a) Snapshot of inter-droplet connection and merging of droplets. (b) Inhibiting inter-droplet connection by jamming one droplet. No merging of droplets.

Published on 29 Juuni 2024. Downloaded on 08/08/2025 06:59:17.

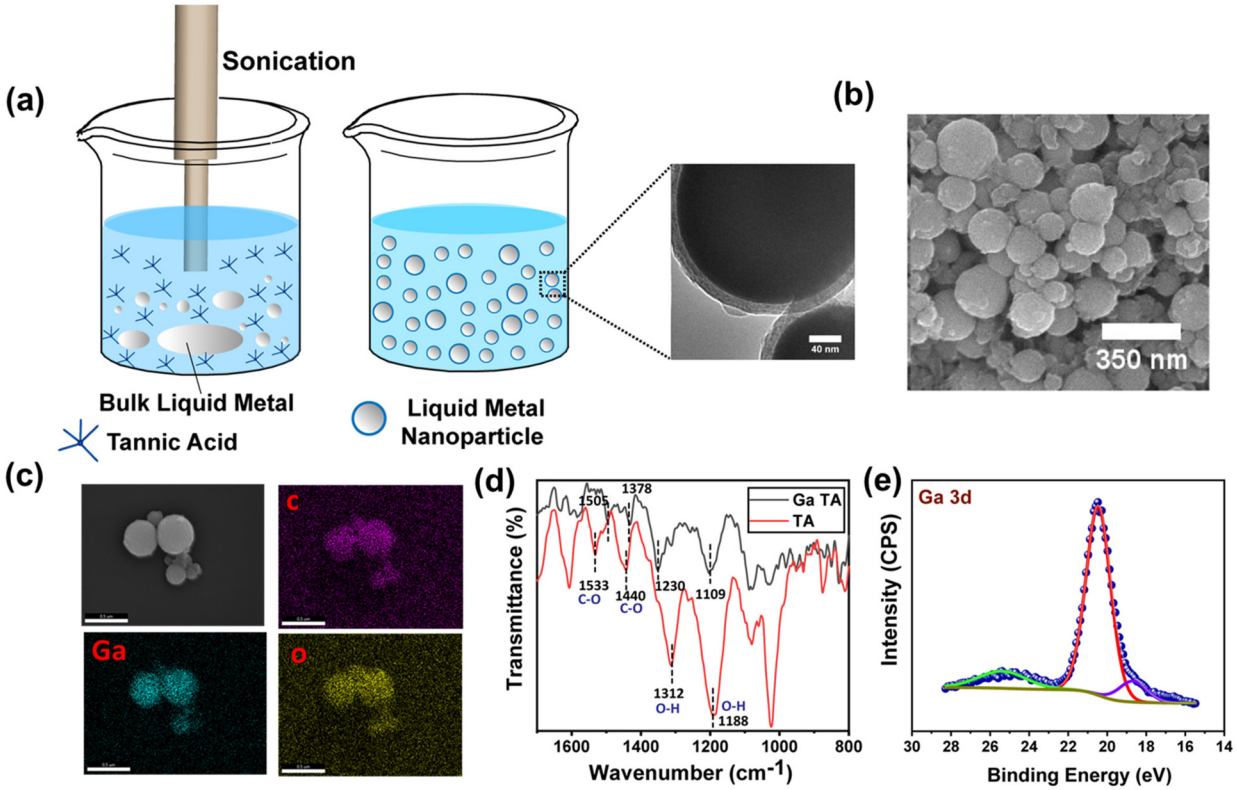

Fig. 5 (a) Synthesis of Ga NP dispersion. (b) SEM image of spherical Ga NPs. (c) EDX analysis of the NPs. (d) FTIR of TA and TA-coated Ga NPs. (e) XPS spectra of Ga NPs representing Ga 3d peaks.

in phenolic O–H bending vibration was observed, and the peaks of TA were shifted from 1312 and 1188 cm^{-1} to 1230 and 1109 cm^{-1}, respectively, in TA-functionalized Ga NPs. This suggests a coordination interaction between Ga^{III} and phenolic groups of TA. X-ray photoelectron spectroscopy (XPS) analysis of the sample (see ESI, Fig. S7a†) showed that the presence of C 1s, O 1s, and Ga 3d peaks is consistent with the composition of TA-coated Ga NPs. The XPS spectra displayed characteristic peaks of the C–O and C═O groups of TA observed at binding energies of 286.4 and 288.8 eV (see ESI, Fig. S7b†), respectively. In particular, the Ga 3d signal at 20.5 eV (Fig. 5e) suggests the possible presence of Ga^{III}, and it matches the literature-reported binding energy of Ga^{III} (19.8 eV) species present as Gallium oxide.

To study the interfacial activity of the freshly prepared NPs, a pendant droplet containing $Fe(acac)_3$ in DCB was created inside an aqueous solution of freshly prepared Ga NPs (Fig. 6a). The droplet crumbled upon extraction of the oil phase, but it recovered to its original shape after reinjection (Fig. 6b). A reduction in interfacial activity was observed due to metal–phenolate complexation, as described earlier. The equilibrium interfacial tension of the complex at 0.1 mM $Fe(acac)_3$ concentration was 26.9 mN m^{-1} when measured after 1200 s. It further decreased to 25.4 mN m^{-1} at a 0.5 mM $Fe(acac)_3$ concentration (Fig. 6c). The control experiment was performed without the addition of any metal salts in the oil phase, and the interfacial tension was found to be higher (29.1 mN m^{-1}) than in the previous measurements. This suggests the metal-mediated crosslinking of TA-functionalized Ga NPs at the oil–water interface. Next, we investigated the surface coverage of the droplet with varying Fe^{III} concentration. It was observed that as the concentration of the metal ions increased, the surface coverage also increased (Fig. 6d). This is due to the higher population of the metal–phenolate complex at the droplet interface.

To demonstrate the liquid-in-liquid sculpting based on previously established chemistry, we fabricated liquid letters composed of TA-functionalized Ga NPs. We expect that the interaction between TA-coated NPs and the metal ions at the liquid–liquid interface enables the molding of liquids. First, the molds of various letters were produced by 3D printing using a commercial 3D printer. The molds were initially pre-wetted with oil containing FeIII ions, followed by the addition of an aqueous solution of TA-coated Ga NPs. The liquid-filled molds were kept aside for 30 minutes for further complexation. Next, we carefully dip the liquid-filled mold into an oil solution containing FeIII ions (Fig. 7a; see also ESI, Fig. S8†). Because the oil phase had a higher density than the aqueous phase, the aqueous feature inside the mold spontaneously floated, thus creating distinctive liquid letters (Fig. 7b). The key to achieving this shape retention was the saturation of the interfacial area by the metal-mediated complexation of Ga NPs. It continuously reduces interfacial tension while creating a close-packed layer of the complex at the interface. Thus, by carefully controlling the properties of the oil and water phases,

 This journal is © The Royal Society of Chemistry 2024

Published on 29 Juuni 2024. Downloaded on 08/08/2025 06:59:17.

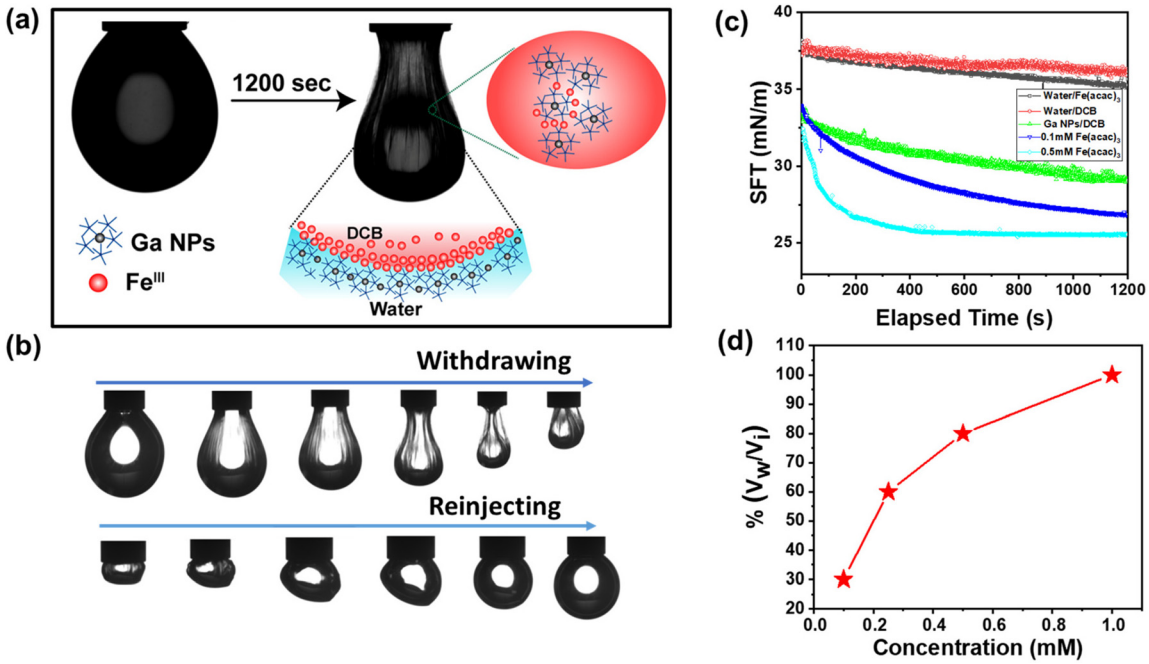

Fig. 6 (a) Schematic representation of TA-coated Ga NP–metal complexation at the oil–water interface. (b) Snapshot showing droplet morphology during withdrawal and reinjection. (c) Time evolution of interfacial tension and (d) surface coverage of Ga NPs with Fe^{III} metal ions (1 mM).

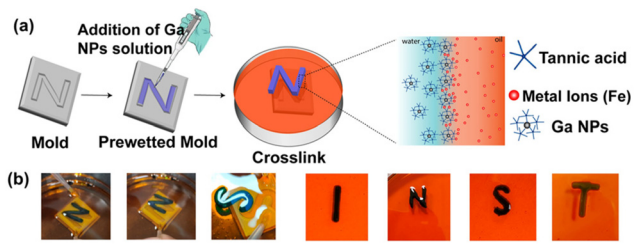

Fig. 7 (a) Schematic of the all-liquid molding process. (b) Snapshots of liquid letters.

as well as the interactions between the ligands and metal ions, we can create and maintain intricate liquid structures within molds.

Metals possess a high abundance of free electrons within their conduction band, contributing to the ohmic-like behavior observed in different Fermi energy metal junctions in the *I–V* characteristic. In low-voltage electronic applications, there should be smooth electronic conduction in both forward and reverse directions without any loss of power due to the threshold voltage. Therefore, it is important to have ohmic contact. The design of all-liquid conducting electrodes is of prime necessity for the development of flexible conducting electrodes using the solid–liquid interface. Fig. 8a depicts an "I"-shaped free-standing structure stabilized by a TA-coated Ga NP network. It was connected to two probes spaced at 1 cm. From this metal–insulator semiconductor-metal platform, Schottky-type behavior was obtained, as shown in Fig. 8b, where a high negative threshold voltage characteristic was observed due to the presence of a thin oxide layer and TA coating on the top Ga NPs as well as the Fermi level mismatch of Ga NPs against metallic probes. At an applied potential of ±10 volt, a maximum current of 200 μA was observed in both maximum forward and reverse biasing. However, while keeping the system at a constant potential of 10 volt, a sharp decrease in conductivity from 200 μA to 17 μA was observed (Fig. 8c) due to severe surface oxidation *via* interfacial resistance-mediated heat formation. Under this condition, a positive voltage sweep of 0 to 10 volt was applied, which revealed a sharp oxidation hump at 1.1 volt, as shown in Fig. 8d. At 10 volt of constant applied potential, severe oxidation of Ga NP occurred, and it resulted in the formation of an insulating oxide layer that was attributed to the reduction in conductivity (see ESI, Fig. S9a†). To remove the non-conducting oxide layer from the surface of Ga NPs, the printed structure was treated with HCl fumes for 10–20 s. No deformation of the structure was observed, and the conductivity gradually increased up to 100 μA, as shown in the same potential window (Fig. 8e).[30] It also signifies the effective way of cleaning the liquid electrode surface *via* simple chemical treatment and reviving its potential activity towards realistic device performance. To understand the electrode potentiality towards the devolvement of flexible liquid-based electronic circuitry, ±1 volt of potential was applied across the liquid Ga-based electrode with a halt time of 5 s at the maximum potential of forward and reverse biases (Fig. 8f). It revealed an unaltered *I–V* response with time that significantly projected towards the reliability of electrode performance. However, with an increasing applied potential of up to ±3 volts, a slight deviation in electrode performance

Published on 29 Juuni 2024. Downloaded on 08/08/2025 06:59:17.

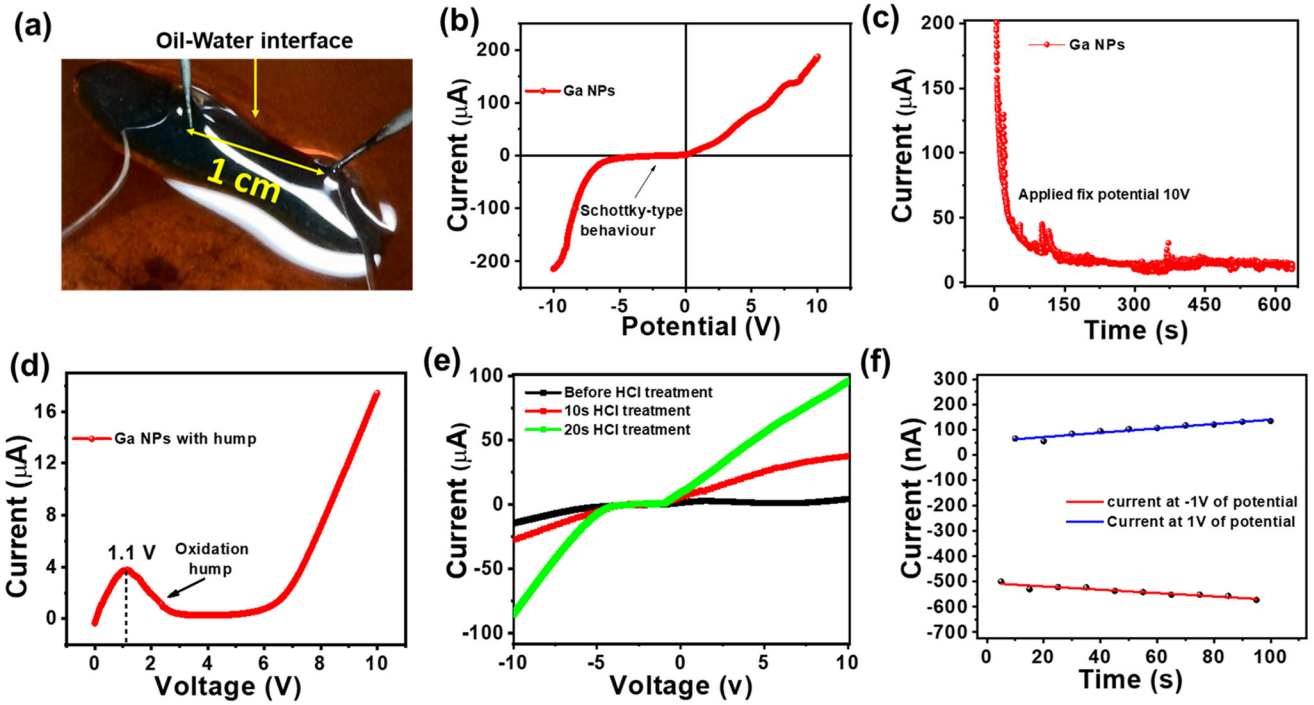

Fig. 8 (a) On the Ga NP surface, two probes are connected and separated by 1 cm. (b) Schottky junction behavior is observed because of the semiconducting nature of this nanoparticle. (c) Conductivity decreases with time at a fixed applied potential of 10 volt. (d) Hump formation at a low potential of 1.1 volt, and after 6 volts, the current is further increased. (e) Current is increased with time after the *in situ* HCl treatment. (f) At ±1 volt of sweep voltage with 5 s current-time characteristic, conductivity remains unaltered.

occurred possibly due to oxide formation (see ESI, Fig. S9b†). Thus, the newly designed Ga-based liquid electrode may find promising applications in low-power electronic circuits.

Conclusions

In summary, we addressed the issue of sculpting liquid Ga NPs. Metal–tannic acid chemistry was utilized at the interface to structure the liquid droplets in various non-equilibrium shapes. We investigated whether the surface coverage of the droplet could be tuned by varying the metal ion concentrations and metal oxidation states. The pH of the solution also played an important role in terms of the stability of the interfacial film. The universal surface adhesion nature of TA was further exploited to functionalize the liquid Ga NPs. The formation of a metal–phenolate network at the interface created liquid Ga NP-based 3D constructs. The *I–V* characteristic curve revealed that the structures were conductive and could be used for low-voltage electronic applications.

Author contributions

DP conceived the idea of the project. RM carried out experimental studies for IFT data, material fabrication and characterization. SD and RM carried out electrical measurements. RM and SD wrote the original draft of the manuscript. AKG and DS helped in material characterization. AS helped in 3D molding. DP and KG supervised the project and helped to structure the manuscript.

Data availability

The data supporting the findings of this study are available on request from the corresponding author.

Conflicts of interest

There are no conflicts to declare.

Acknowledgements

DP acknowledges the financial support from SERB-DST (CRG/2022/004595). KG acknowledges the financial support from Ministry of Textiles [grant no: 2/3/2021-NTTM (Pt.)].

References

1 M. D. Bartlett, *Nat. Mater.*, 2021, **20**, 714–715.
2 M. D. Dickey, *Adv. Mater.*, 2017, **29**, 1606425.
3 R. Lin, H.-J. Kim, S. Achavananthadith, Z. Xiong, J. K. Lee, Y. L. Kong and J. S. Ho, *Nat. Commun.*, 2022, **13**, 2190.

 This journal is © The Royal Society of Chemistry 2024

Published on 29 Juuni 2024. Downloaded on 08/08/2025 06:59:17.

4 K. Karuppasamy, J. Theerthagiri, D. Vikraman, C.-J. Yim, S. Hussain, R. Sharma, T. Maiyalagan, J. Qin and H.-S. Kim, *Polymers*, 2020, **12**, 918.
5 P. Won, S. Jeong, C. Majidi and S. H. Ko, *iScience*, 2021, **24**, 102698.
6 J. M. R. Tan, Y. Farraj, A. Kamyshny and S. Magdassi, *ACS Appl. Electron. Mater.*, 2023, **5**, 1376–1393.
7 Q. Gui, Y. He and Y. Wang, *Adv. Electron. Mater.*, 2021, **7**, 2000780.
8 Y. G. Park, G. Y. Lee, J. Jang, S. M. Yun, E. Kim and J. U. Park, *Adv. Healthcare Mater.*, 2021, **10**, 2002280.
9 J. Yang, W. Cheng and K. Kalantar-Zadeh, *Proc. IEEE*, 2019, **107**, 2168–2184.
10 G. Li, M. Zhang, S. Liu, M. Yuan, J. Wu, M. Yu, L. Teng, Z. Xu, J. Guo and G. Li, *Nat. Electron.*, 2023, **6**, 154–163.
11 M. Li, Y. Wu, L. Zhang, H. Wo, S. Huang, W. Li, X. Zeng, Q. Ye, T. Xu and J. Luo, *Nanoscale*, 2019, **11**, 5441–5449.
12 G. Lu, E. Ni, Y. Jiang, W. Wu and H. Li, *Small*, 2023, 2304147.
13 H. Wang, S. Chen, X. Zhu, B. Yuan, X. Sun, J. Zhang, X. Yang, Y. Wei and J. Liu, *Matter*, 2022, **5**, 2054–2085.
14 W. Babatain, M. S. Kim and M. M. Hussain, *Adv. Funct. Mater.*, 2023, 2308116.
15 S. Chen, H.-Z. Wang, R.-Q. Zhao, W. Rao and J. Liu, *Matter*, 2020, **2**, 1446–1480.
16 J. Ma, F. Krisnadi, M. H. Vong, M. Kong, O. M. Awartani and M. D. Dickey, *Adv. Mater.*, 2023, **35**, 2205196.
17 S. Liang, J. Yang, F. Li, S. Xie, N. Song and L. Hu, *RSC Adv.*, 2023, **13**, 26650–26662.
18 R. Zhao, R. Guo, X. Xu and J. Liu, *ACS Appl. Mater. Interfaces*, 2020, **12**, 36723–36730.
19 M. Cui, T. Emrick and T. P. Russell, *Science*, 2013, **342**, 460–463.
20 C. Agashe, R. Varshney, R. Sangwan, A. K. Gill, M. Alam and D. Patra, *Langmuir*, 2022, **38**, 8296–8303.
21 S.-Y. Tang and R. Qiao, *Acc. Mater. Res.*, 2021, **2**, 966–978.
22 M. A. Rahim, S. L. Kristufek, S. Pan, J. J. Richardson and F. Caruso, *Angew. Chem., Int. Ed.*, 2019, **58**, 1904–1927.
23 J. Saiz-Poseu, J. Mancebo-Aracil, F. Nador, F. Busqué and D. Ruiz-Molina, *Angew. Chem., Int. Ed.*, 2019, **58**, 696–714.
24 B. J. Kim, S. Han, K. B. Lee and I. S. Choi, *Adv. Mater.*, 2017, **29**, 1700784.
25 S. Cakar and M. Özacar, *J. Photochem. Photobiol., A*, 2019, **371**, 282–291.
26 S. YeongáHan, *Chem. Commun.*, 2020, **56**, 13748–13751.
27 B. N. Ganguly, V. Verma, D. Chatterjee, B. Satpati, S. Debnath and P. Saha, *ACS Appl. Mater. Interfaces*, 2016, **8**, 17127–17137.
28 W. R. Loewenstein, *Physiol. Rev.*, 1981, **61**, 829–913.
29 A. Yamaguchi, Y. Mashima and T. Iyoda, *Angew. Chem., Int. Ed.*, 2015, **54**, 12809–12813.
30 K. Y. Kwon, V. K. Truong, F. Krisnadi, S. Im, J. Ma, N. Mehrabian, T.-I. Kim and M. D. Dickey, *Adv. Intell. Syst.*, 2021, **3**, 2000159.